Front. Phys. 13(3), 138104 (2018)
https://doi.org/10.1007/s11467-018-0760-8

RESEARCH ARTICLE

SiP monolayers: New 2D structures of group IV–V compounds for visible-light photohydrolytic catalysts

Zhinan Ma (马志楠)[1,2,†], **Jibin Zhuang** (庄吉彬)[1], **Xu Zhang** (张旭)[3], **Zhen Zhou** (周震)[2,3,‡]

[1] *School of Science, North University of China, Taiyuan 030051, China*
[2] *Key Laboratory of Advanced Energy Materials Chemistry (Ministry of Education), Nankai University, Tianjin 300071, China*
[3] *School of Materials Science and Engineering, National Institute for Advanced Materials, Computational Centre for Molecular Science, Institute of New Energy Material Chemistry, Collaborative Innovation Center of Chemical Science and Engineering (Tianjin), Nankai University, Tianjin 300350, China*
Corresponding authors. E-mail: [†]*mazhinan@163.com*, [‡]*zhouzhen@nankai.edu.cn*
Received December 11, 2017; accepted January 14, 2018

Because of graphene and phosphorene, two-dimensional (2D) layered materials of group IV and group V elements arouse great interest. However, group IV–V monolayers have not received due attention. In this work, three types of SiP monolayers were computationally designed to explore their electronic structure and optical properties. Computations confirm the stability of these monolayers, which are all indirect-bandgap semiconductors with bandgaps in the range 1.38–2.21 eV. The bandgaps straddle the redox potentials of water at pH = 0, indicating the potential of the monolayers for use as water-splitting photocatalysts. The computed optical properties demonstrate that certain monolayers of SiP 2D materials are absorbers of visible light and would serve as good candidates for optoelectronic devices.

Keywords graphene, phosphorene, group IV–V monolayers, photocatalytic water splitting, SiP 2D materials

PACS numbers 73.21.At, 73.22.-f, 81.07.-b, 88.80.-q

1 Introduction

Because of their unique physical and chemical properties, ultrathin two-dimensional (2D) materials have aroused much interest in the past decade [1, 2]. Since its exfoliation from graphite in 2004, the 2D structure of graphene has become widely known for its one-atom thickness [3]. Since then, *h*-BN, MoS_2, phosphorene, MXene, g-CN, and other 2D structures have also emerged in mono- or a-few-layer forms [4–16]. More and more investigations of these materials have revealed intriguing properties and potential for electronic, optical, and other device applications. For example, graphene displays superior thermal conductivity, and high carrier mobility and Young's modulus [17, 18]. The structure of *h*-BN is similar to that of graphene with high transparency [19]. MoS_2 monolayer is considered as a low-consumption transistor [20]. Recently, ultrastrong optical non-linearity has been observed in the MoS_2 monolayer, endowing it with device application characteristics [21, 22]. Phosphorene is a semiconductor with a natural bandgap suitable for applications in electronics and optoelectronics [23, 24]. Based on different terminal groups and transition elements, MXene materials exhibit metallic to semiconducting behavior [25]. Metal-free magnetism of g-C_4N_3 and enhanced catalytic activity for H_2 release over g-C_3N_4 suggest excellent properties of graphitic carbon nitride [26, 27].

Since many properties of the 2D materials are superior to those of the bulk, designing and synthesizing similar structures are indeed increasingly promising. Replacing the elements in the known 2D structures by the same group elements is a common practice. For example, when the C atoms are replaced by Si or Ge in the base of graphene structure, a set of new 2D group IV materials, namely silicene and germanene have emerged [28, 29]. In

*Special Topic: Inorganic Two-Dimensional Nanomaterials (Eds. Changzheng Wu & Xiaojun Wu).

© Higher Education Press and Springer-Verlag GmbH Germany, part of Springer Nature 2018

the MoS_2 monolayer, Mo or S could be replaced by W or Se, respectively [30–32], thus breeding the series of MoS_2, WS_2, $MoSe_2$, and WSe_2 monolayers. Following the success of phosphorene, arsenene and antimonene were also explored as 2D group V monolayers [33–36]. Investigations on such 2D materials are abundant; however, despite many published reports on g-CN layers, studies of the IV–V 2D materials are rather scarce [37–40]. Silicon phosphide (SiP) falls under this category. Bulk SiP has been synthesized experimentally, and the stability and electronic properties of the SiP monolayers have been derived computationally [38, 41]. In these investigations, a g-Si_3P_3 structure was designed with a direct bandgap of 1.93 eV [37]. Zhang *et al.* [38] suggested that the SiP monolayer exfoliated from the bulk is stable with a semiconducting nature. The PSi_3 layer is also a stable structure with a narrow bandgap [39]. All these results imply that designing new SiP monolayers is significant to realize materials with unique properties and extend the range of group IV–V 2D materials.

Motivated by the experimental developments and theoretical investigations, we designed three types of SiP monolayers from first-principle calculations. The SiP monolayer has a hexagonal primitive cell, different from the orthogonal layered cell structure of the bulk SiP obtained from experiment [41]. The stability of the optimized monolayers could be confirmed computationally. Further, evaluation of the band structures and absorption features of the monolayers indicated the possibility of using them as visible-light water-splitting photocatalysts. The imaginary part of the dielectric function (ε_2) was evaluated to supplement the data and assess the light absorption capability of these materials for possible application in electronic and optical devices.

2 Computational details

Computations were performed within the MedeA® software environment [42]. The generalized gradient approximation (GGA) for exchange correlation functional was employed, and the monolayer structures were optimized with the Perdew–Burke–Ernzerhof (PBE) exchange-correlation functional [43]. The cutoff energy was set to 550 eV. The Heyd–Scuseria–Ernzerhof 06 (HSE06) hybrid functional was used to obtain an accurate description of the electronic band structures [44]. For all the electronic property computations, a mesh of $11 \times 11 \times 1$ k-points was used for sampling the Brillouin zone. Ab initio molecular dynamics (AIMD) simulation was employed to confirm the stability of the SiP structure. The AIMD simulation in a NVT ensemble was performed for 10 ps with a time step of 2.0 fs. The Nosé–Hoover method was adopted for temperature control [45].

For the computation of the phonon dispersion spectrum, CASTEP code was employed for PBE computations based on the density functional perturbation theory (DFPT) [46]. The cutoff energy was chosen as 480 eV and a k-mesh of $8 \times 8 \times 1$ was used. All computations were performed in supercells with a vacuum space larger than 15 Å above and below the monolayers.

3 Results and discussion

In the first step, three SiP monolayers were designed, as shown in Fig. 1. The three SiP monolayers labeled α-, β-, and γ-SiP have the same basic structure. α- and β-SiP are mirror-symmetry structures. γ-SiP does not have mirror-symmetry but has one Si and one P positioned inside or outside. Because of similar basic structure and nature of elements in the three monolayers, the lattice parameters are also similar, as shown in Table 1.

To investigate the chemical structures of α-, β-, and γ-SiP further, the bond lengths and bond angles were analyzed. In α-SiP, there are two types of bonds, namely the Si–P bond (2.32 Å) and P–P bond (2.27 Å). For β-SiP, no P–P bond exists. The bonds in β-SiP are the Si–P bond (2.28 Å) and Si–Si bond (2.37 Å). For γ-SiP, the P/Si ratio within the structure (P(i) and Si(i)) and on the terminals (P(t) and Si(t)) is a factor to be considered. As a result, it possessed three types of Si–P bonds, namely the Si(t)–P(i) bond (2.33 Å), Si(i)–P(i) bond (2.28 Å), and Si(i)–P(t) bond (2.27 Å). Bond lengths of all the three monolayers were in the range 2.27–2.37 Å, which meant that they are closely similar.

The bond angles are shown in Fig. 1. The nature of the chemical environment causes variations in the bond angles. When the Si atoms are on top, as shown in Figs. 1(a) and (c), the values of bond angles on the surface are approximately 98°. However, when P atoms are on top, as shown in Figs. 1(b) and (d), the bond angles are higher, at approximately 101.9°. Obviously, the bond angles in the interior of the structure are larger than those on the surface. The interior bond angles are formed by the atoms located at the angular vertex. The bond angles with the P atom on the angular vertex are larger than those with the Si atom on the vertex.

Table 1 Lattice parameter, cohesive energy and bandgap of the α-, β-, and γ-SiP monolayers.

Monolayer parameter	α-SiP	β-SiP	γ-SiP
Lattice parameter a (Å)	3.52	3.53	3.53
E_{coh} (eV)	3.89	4.21	4.08
Bandgap (eV)	1.38	2.21	2.03

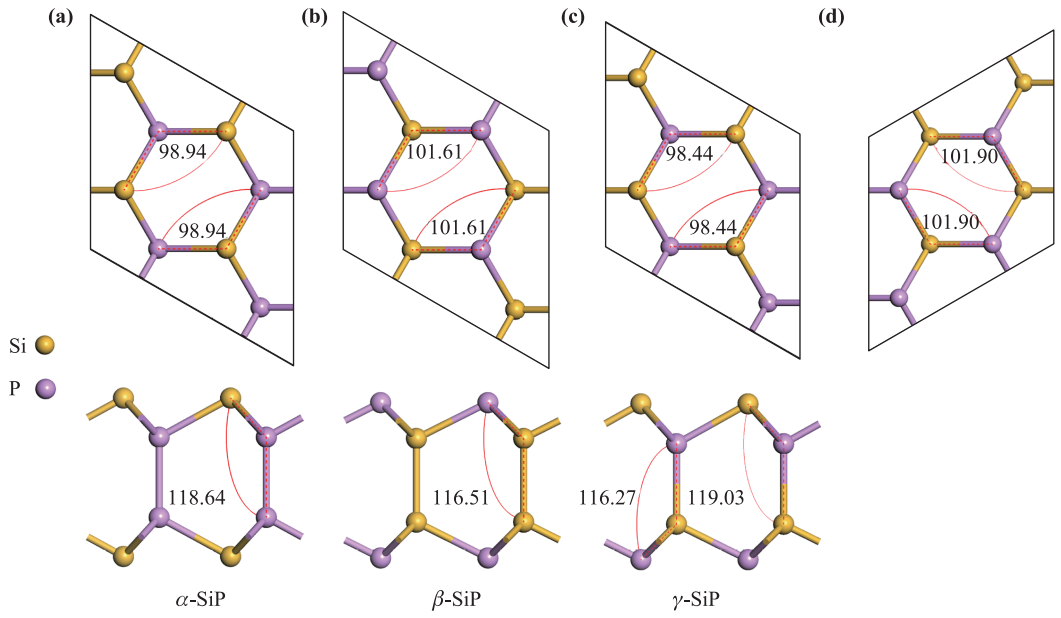

Fig. 1 **(a)** Top and side views of the α-SiP monolayer in 2×2 supercells drawn with the values of bond angles. **(b)** Top and side views of the β-SiP monolayer in 2×2 supercells. **(c)** Top and side views of the γ-SiP monolayers in 2×2 supercells. **(c)** and **(d)** are the views of the γ-SiP surfaces with Si or P atom on the top, respectively.

Although an optimum geometry for the α-, β-, and γ-SiP monolayers was obtained through computations, it was necessary to confirm the stability of these structures. In Fig. 2(a), the phonon dispersion spectra are presented along the high-symmetry points in the Brillouin zone, including those at G(0,0,0), K(−0.333,0.667,0), and M(0,0.5,0). There is no imaginary component of frequency observed in any of the dispersion spectra which demonstrates the kinetic stability of the phonon frequencies. Further, a series of AIMD simulations were performed at 1000 K for 10 ps to confirm the thermal stability. The results are shown in Fig. 3. The overall structural integrity is maintained for all the SiP monolayers although some of the bonds are found to be broken. Besides the phonon dispersion spectra and AIMD simulation, the cohesive energy (E_{coh}) was calculated from the equation: $E_{\mathrm{coh}} = (nE_{\mathrm{Si}} + nE_{\mathrm{p}} - E_{\mathrm{SiP}})/(2n)$. Here, n refers to the quantity of an element in a cell. The cohesive energies of all the SiP monolayers are in the range 3.89–4.21 eV as shown in Table 1. In comparison, the cohesive energies of silicene and phosphorene are 3.98 and 3.24 eV, respectively, obtained using the same method. The values of SiP monolayers are comparable to those of silicene. All these calculations reveal that the monolayers are stable configurations and it is possible to realize them in practice.

To examine the electronic structure of the α-, β-, and γ-SiP monolayers, we adopted the HSE06 hybrid functional for computations of the band structures. The results are illustrated in Fig. 2(b). The calculated values of the bandgaps are included in Table 1. It can be seen in Fig. 2(b) that all the monolayers are indirect bandgap semiconductors with the conduction band minima (CBM) at point M. For the α- and γ-SiP, the valence band maxima (VBM) are located at point K and the bandgaps are deduced as 1.38 and 2.03 eV, respectively. However, the VBM of the β-SiP monolayer lies between the points G and K. Compared with α-, and γ-SiP, the β-SiP monolayer reveals a larger bandgap of 2.21 eV.

Additionally, the effective mass was calculated for all the monolayers from the expression $m^* = \hbar^2(\partial^2 E(k)/\partial k^2)^{-1}$. The constructed unit cell configurations of the α-, β-, or γ-SiP monolayers in the orthogonal supercell and the corresponding band structures (illustrated in Fig. 4) were analyzed to estimate the effective mass (m^*) along the x- and y-directions. The calculated values of effective mass are tabulated in Table 2. For the β-SiP, the value of m* for electrons along the y-direction is smaller than that along the x-direction and also that of holes along the x- and y-directions. In the case of γ-SiP,

Table 2 Effective mass $|m^*|$ (m_e) of $\alpha\gamma$ lectrons and holes along the x- and y-direction in α-, β-, and γ-SiP monolayers.

Charge carrier in SiP monolayer	Effective mass $\lvert m^*\rvert$ (m_e)		
	α-SiP	β-SiP	γ-SiP
Hole (x)	0.53	1.90	2.20
Electron (x)	0.26	1.66	2.08
Hole (y)	0.29	2.35	0.62
Electron (y)	0.72	0.13	0.12

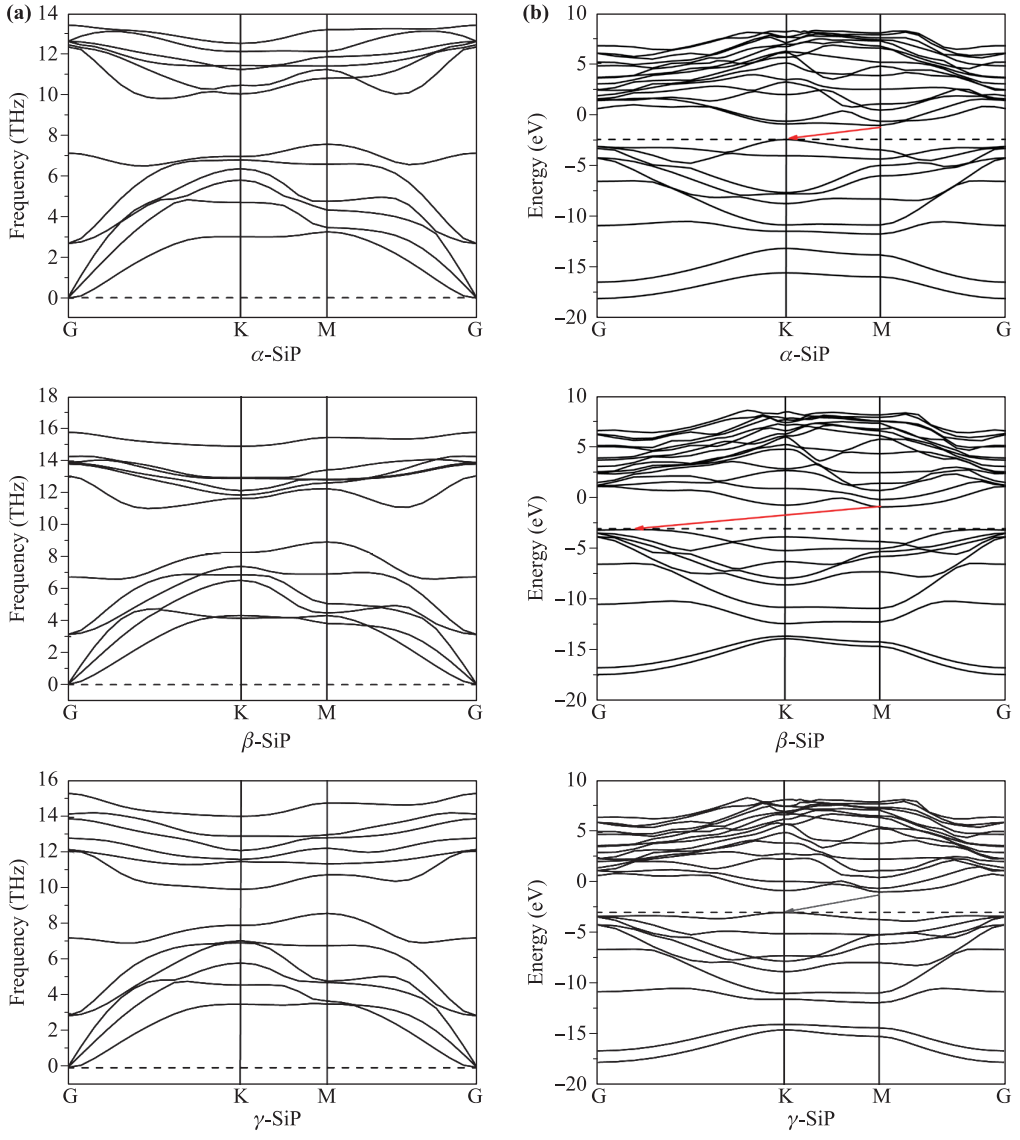

Fig. 2 **(a)** Phonon dispersion spectra of α-, β-, and γ-SiP monolayers. **(b)** Band structures of α-, β-, and γ-SiP monolayers. Dashed line in (b) represents the valence band maxima (VBM).

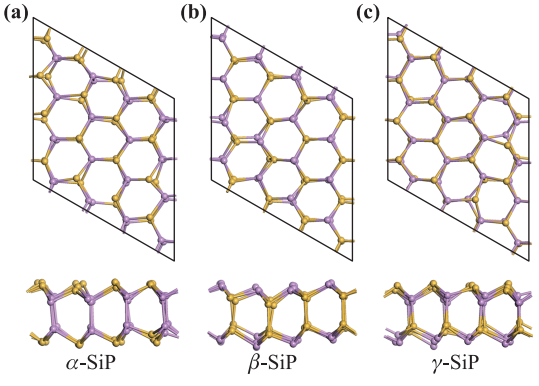

Fig. 3 The equilibrium structures for α-, β-, and γ-SiP monolayers at 1000 K.

the values of m^* for both electrons and holes along the x-direction are larger than those along the y-direction. Except in the case of electrons in the y-direction, α-SiP possesses the lowest values of m^* among all three monolayers.

For a better understanding of the electronic structure of the monolayers, we analyzed the plots of the partial density of states (PDOS), which are shown in Fig. 5. For the monolayers α- and β-SiP, the main VBM originates from the p orbitals of P and Si atoms. In the case of β-SiP, the s and p orbitals of the two elements determine the main CBM. However, for α-SiP, the peak intensity of the s orbital of the Si atoms located in the CBM is small. The situation in the case of γ-SiP is complicated

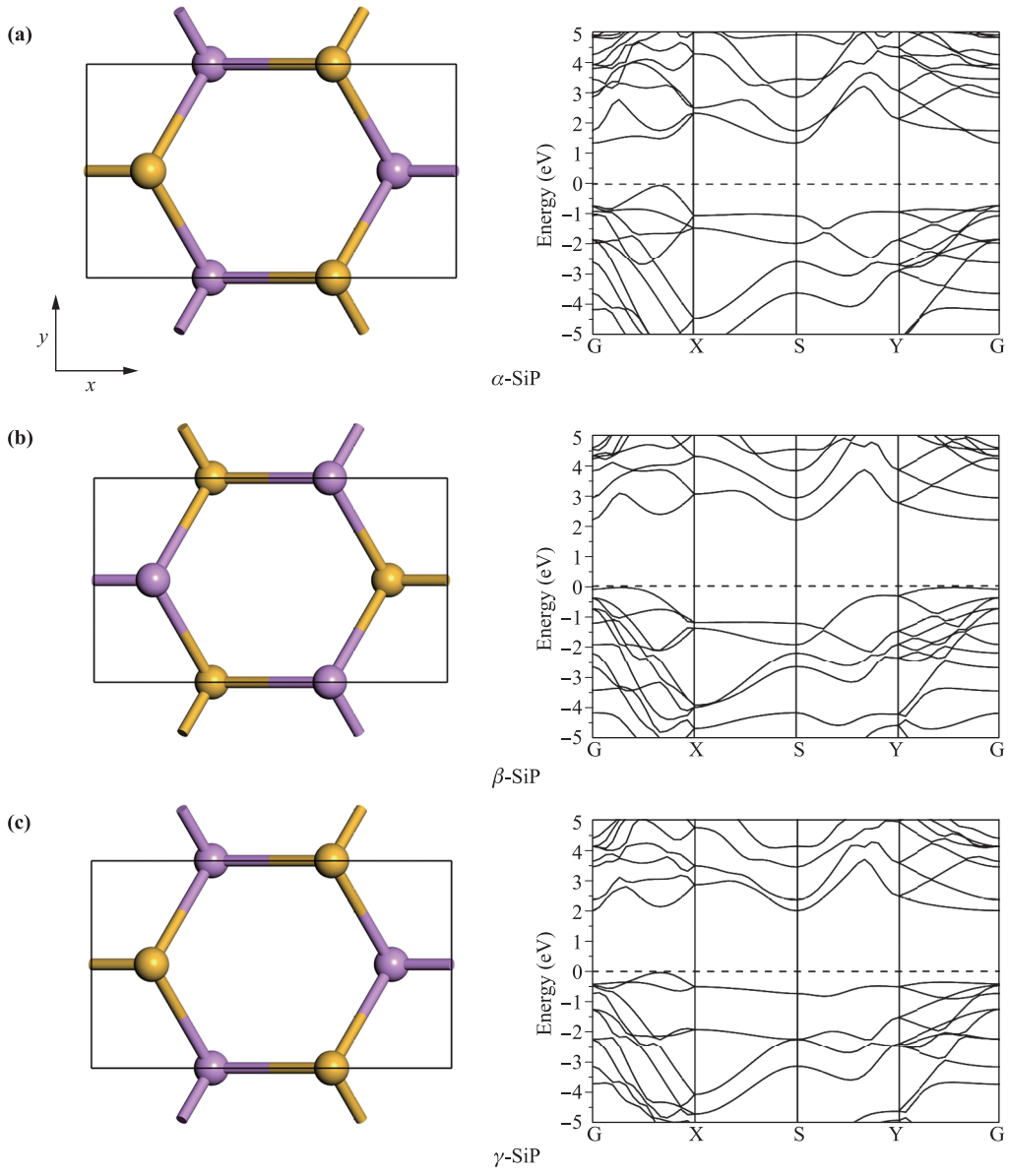

Fig. 4 Constructed unit cell (orthogonal) configurations of the α-, β-, or γ-SiP monolayers and the corresponding band structures.

because of the symmetry of its structure. As shown in Fig. 5(c), the major portion of CBM for γ-SiP is derived from s/p orbitals of Si and P on the terminal. However, only the p orbitals of P and the s/p orbitals of Si atoms on the terminal influence the VBM.

Further, the suitability of the monolayer as a photocatalyst for water splitting under visible-light irradiation was examined. The potentials for oxidation and reduction are pH dependent [47, 48]. The reduction/oxidation potentials are described by the equations

$$E^{red}_{\mathrm{H^+/H_2}} = -4.44\ \mathrm{eV} + \mathrm{pH} \times 0.059\ \mathrm{eV},$$
$$E^{\mathrm{ox}}_{\mathrm{O_2/H_2O}} = -5.67\ \mathrm{eV} + \mathrm{pH} \times 0.059\ \mathrm{eV}.$$

The location of the band edges of the α-, β-, and γ-SiP monolayers are shown in Fig. 6. It can be seen that the conduction band minima (CBM) of all the monolayers are positioned above the hydrogen evolution potential (reduction of H^+/H_2) for the condition, pH = 7. However, at pH = 0, the VBM of all the monolayers lie below the oxygen evolution potential (oxidation of O_2/H_2O). In fact, the conduction and valence band edges straddle the redox potentials of water so as to thermodynamically favor both reactions to take place simultaneously. This means that at a suitable pH condition all the monolayer materials described in this study can potentially be used as water-splitting catalysts.

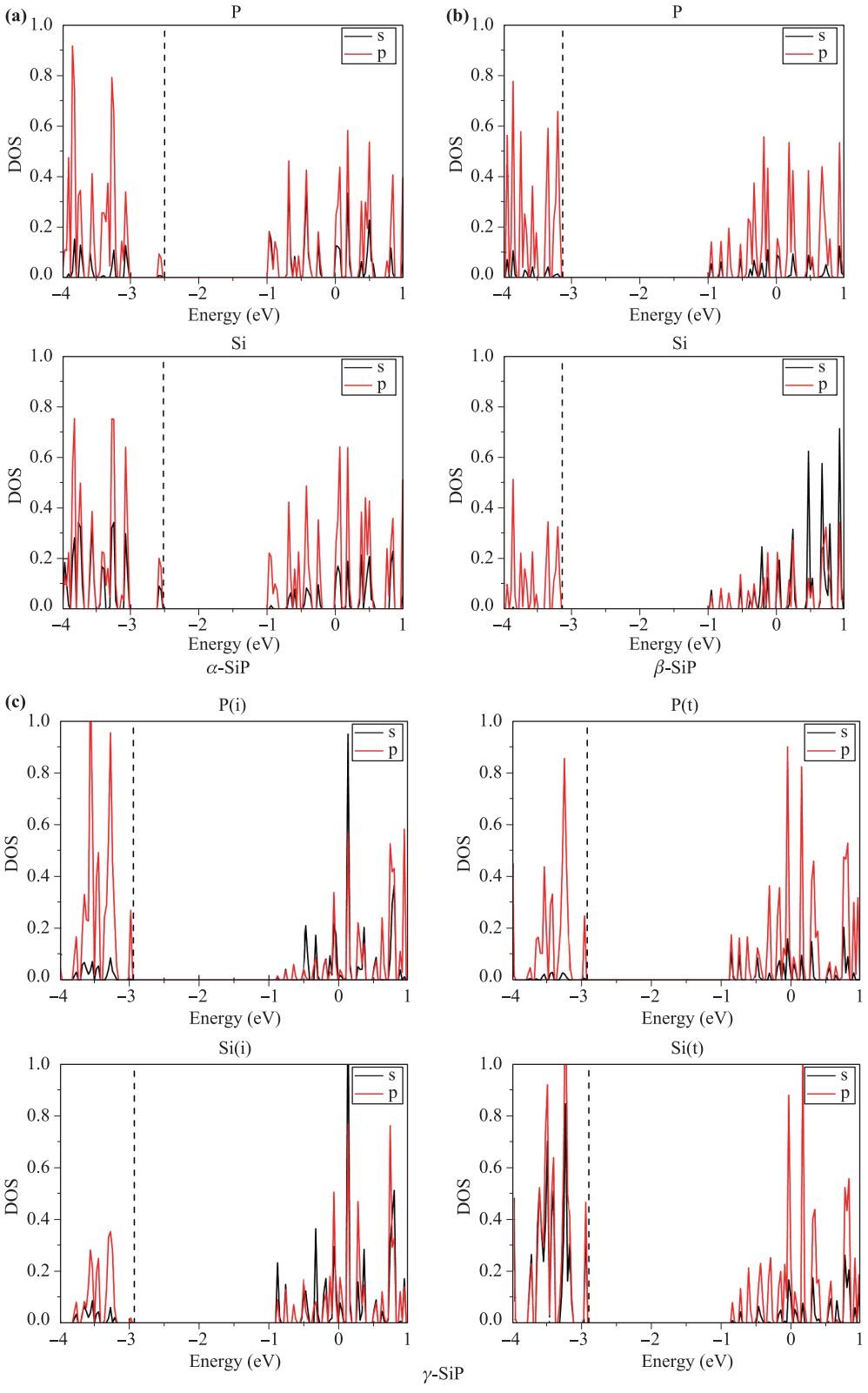

Fig. 5 Calculated partial density of states (PDOS) for the three monolayer structures. **(a)** α-SiP. **(b)** β-SiP. **(c)** γ-SiP. Dashed line is the location of VBM. P/Si inside the structure [P(i) and Si(i)] and on the terminals [P(t) and Si(t)] are partly considered for γ-SiP.

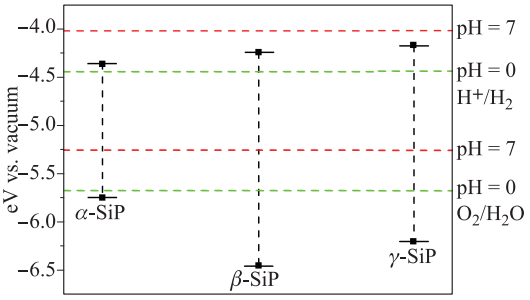

Fig. 6 The location of calculated VBM and CBM of the SiP monolayers shown as bars with black squares. The redox potentials for the catalytic splitting of water at pH = 0 (green dashed lines) and pH = 7 (red dashed lines) are shown for comparison.

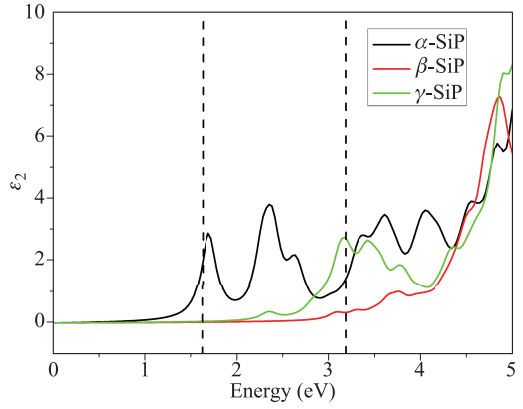

Fig. 7 Variation in the imaginary part of the dielectric constant (ε_2) with photon energy for the three SiP monolayers obtained from the average of x, y, and z polarization vectors. The area between the dashed vertical lines is the energy range of visible light (1.64 to 3.19 eV).

To investigate the efficiency of light absorption by these materials, the optical absorption characteristics were evaluated in the visible spectral region. We calculated the imaginary part of the dielectric constant (ε_2) and plotted the same as a function of photon energy which is shown in Fig. 7. The imaginary part was determined using the following equation:

$$\varepsilon^{(2)}_{\alpha\beta}(\omega) = \frac{4\pi^2 e^2}{\Omega} \lim_{q\to 0} \frac{1}{q^2} \sum_{c,v,k} 2w_k \delta(\varepsilon_{ck} - \varepsilon_{vk} - \omega) \times \langle u_{ck+e_\alpha q} | u_{vk} \rangle \langle u_{ck+e_\beta q} | u_{vk} \rangle^*.$$

Here, the indices c and v refer to the conduction and valence band states, respectively, and u_{ck} is the cell periodic component of the orbitals at the k-point K. As shown in Fig. 7, the α-SiP displays significant absorption (black line) in the visible region (resulting from a relatively small bandgap) with two peaks discernible at 1.69 and 2.53 eV. On the contrary, the absorption of visible light was very weak (represented by the red line) in the β-SiP monolayer consequent to a larger bandgap (which is incidentally the largest among all three monolayers). In the case of γ-SiP, a broad absorption peak (green line) appears at the far edge (3.2 eV) of the visible spectral range.

4 Conclusion

In conclusion, three monolayer structures, namely α-, β-, and γ-SiP from group IV–V elements were constructed and their structural and electronic properties were investigated by DFT calculations. The phonon dispersion spectra and AIMD simulations indicate that all the structures are stable. These monolayers possess indirect bandgaps in the range of 1.38–2.21 eV. Further, it was shown that the bandgaps of all the monolayers straddle the redox potentials of water which is expected to facilitate photocatalytic water splitting. This implies that at a suitable pH condition these materials serve as good candidates for water-splitting photocatalysts. The imaginary part of the dielectric constant was calculated in all the monolayers and its variation and features were analyzed as a function of photon energy. A relatively large absorption in the visible light wavelength region indicated that the; α- and γ-SiP monolayers have potential for application in electronic and optical devices.

Acknowledgements This work was supported by the National Science Foundation of China (Grant No. 21503195), Natural Science Foundation of Shanxi Province (2015021044), and Open Research Fund of Key Laboratory of Advanced Energy Materials Chemistry (Ministry of Education), Nankai University in China.

References and notes

1. Q. Tang and Z. Zhou, Graphene-analogous low-dimensional materials, *Prog. Mater. Sci.* 58(8), 1244 (2013)
2. Q. Tang, Z. Zhou, and Z. Chen, Innovation and discovery of graphene-like materials via density-functional theory computations, *Wiley Interdiscip. Rev. Comput. Mol. Sci.* 5(5), 360 (2015)
3. K. S. Novoselov, A. K. Geim, S. V. Morozov, D. Jiang, Y. Zhang, S. V. Dubonos, I. V. Grigorieva, and A. A. Firsov, Electric field effect in atomically thin carbon films, *Science* 306(5696), 666 (2004)
4. D. Pacilé, J. C. Meyer, C. O. Girit, and A. Zettl, The two-dimensional phase of boron nitride: Few-atomic-layer sheets and suspended membranes, *Appl. Phys. Lett.* 92(13), 133107 (2008)

5. Y. Lin, T. V. Williams, and J. W. Connell, Soluble, exfoliated hexagonal boron nitride nanosheets, *J. Phys. Chem. Lett.* 1(1), 277 (2010)
6. R. V. Gorbachev, I. Riaz, R. R. Nair, R. Jalil, L. Britnell, B. D. Belle, E. W. Hill, K. S. Novoselov, K. Watanabe, T. Taniguchi, A. K. Geim, and P. Blake, Hunting for monolayer boron nitride: Optical and Raman signatures, *Small* 7(4), 465 (2011)
7. C. Lee, H. Yan, L. E. Brus, T. F. Heinz, J. Hone, and S. Ryu, Anomalous lattice vibrations of single- and few-layer MoS_2, *ACS Nano* 4(5), 2695 (2010)
8. K. F. Mak, C. Lee, J. Hone, J. Shan, and T. F. Heinz, Atomically thin MoS_2: A new direct-gap semiconductor, *Phys. Rev. Lett.* 105(13), 136805 (2010)
9. L. Li, Y. Yu, G. J. Ye, Q. Ge, X. Ou, H. Wu, D. Feng, X. H. Chen, and Y. Zhang, Black phosphorus field-effect transistors, *Nat. Nanotechnol.* 9(5), 372 (2014)
10. H. Liu, A. T. Neal, Z. Zhu, Z. Luo, X. Xu, D. Tománek, and P. D. Ye, Phosphorene: An unexplored 2D semiconductor with a high hole mobility, *ACS Nano* 8(4), 4033 (2014)
11. E. S. Reich, Phosphorene excites materials scientists, *Nature* (7486), 19 (2014)
12. M. Naguib, M. Kurtoglu, V. Presser, J. Lu, J. J. Niu, M. Heon, L. Hultman, Y. Gogotsi, and M. W. Barsoum, Two-dimensional nanocrystals produced by exfoliation of Ti_3AlC_2, *Adv. Mater.* 23(37), 4248 (2011)
13. M. Naguib, O. Mashtalir, J. Carle, V. Presser, J. Lu, L. Hultman, Y. Gogotsi, and M. W. Barsoum, Two-dimensional transition metal carbides, *ACS Nano* 6(2), 1322 (2012)
14. X. Zhang, Z. Zhang, and Z. Zhou, MXene-based materials for electrochemical energy storage, *J. Energy Chem.* 27(1), 73 (2017)
15. X. Zhang, X. Zhao, D. Wu, Y. Jing, and Z. Zhou, $MnPSe_3$ monolayer: A promising 2D visible-light photohydrolytic catalyst with high carrier mobility, *Adv. Sci.* 3(10), 1600062 (2016)
16. J. S. Lee, X. Wang, H. Luo, and S. Dai, Fluidic carbon precursors for formation of functional carbon under ambient pressure based on ionic liquids, *Adv. Mater.* 22(9), 1004 (2010)
17. A. A. Balandin, S. Ghosh, W. Bao, I. Calizo, D. Teweldebrhan, F. Miao, and C. N. Lau, Superior thermal conductivity of single-layer graphene, *Nano Lett.* 8(3), 902 (2008)
18. C. Lee, X. Wei, J. W. Kysar, and J. Hone, Measurement of the elastic properties and intrinsic strength of monolayer graphene, *Science* 321(5887), 385 (2008)
19. Y. Lin and J. W. Connell, Advances in 2D boron nitride nanostructures: Nanosheets, nanoribbons, nanomeshes, and hybrids with graphene, *Nanoscale* 4(22), 6908 (2012)
20. B. Radisavljevic, A. Radenovic, J. Brivio, V. Giacometti, and A. C. Kis, Single-layer MoS_2 transistors, *Nat. Nanotechnol.* 6(3), 147 (2011)
21. S. J. R. Tan, I. Abdelwahab, Z. Ding, X. Zhao, T. Yang, G. Z. J. Loke, H. Lin, I. Verzhbitskiy, S. M. Poh, H. Xu, C. T. Nai, W. Zhou, G. Eda, B. Jia, and K. P. Loh, Chemical stabilization of 1T′ phase transition metal dichalcogenides with giant optical Kerr nonlinearity, *J. Am. Chem. Soc.* 139(6), 2504 (2017)
22. A. SäynSätjoki, L. Karvonen, H. Rostami, A. Autere, S. Mehravar, A. Lombardo, R. A. Norwood, T. Hasan, N. Peyghambarian, H. Lipsanen, K. Kieu, A. C. Ferrari, M. Polini, and Z. Sun, Ultra-strong nonlinear optical processes and trigonal warping in MoS_2 layers, *Nat. Commun.* 8(1), 893 (2017)
23. J. S. Qiao, X. H. Kong, Z. Hu, F. Yang, and W. Ji, High-mobility transport anisotropy and linear dichroism in few-layer black phosphorus, *Nat. Commun.* 5, 4475 (2014)
24. H. Liu, Y. C. Du, Y. X. Deng, and P. D. Ye, Semiconducting black phosphorus: Synthesis, transport properties and electronic applications, *Chem. Soc. Rev.* 44(9), 2732 (2015)
25. M. Khazaei, M. Arai, T. Sasaki, C. Y. Chung, N. S. Venkataramanan, M. Estili, Y. Sakka, and Y. Kawazoe, Novel electronic and magnetic properties of two-dimensional transition metal carbides and nitrides, *Adv. Funct. Mater.* 23(17), 2185 (2013)
26. A. Du, S. Sanvito, and S. C. Smith, First-principles prediction of metal-free magnetism and intrinsic half-metallicity in graphitic carbon nitride, *Phys. Rev. Lett.* 108(19), 197207 (2012)
27. X. Zhao, Z. Ma, D. Wu, X. Zhang, Y. Jing, and Z. Zhou, Computational study of catalytic effect of C_3N_4 on H_2 release from complex hydrides, *Int. J. Hydrogen Energy* 40(29), 8897 (2015)
28. S. Cahangirov, M. Topsakal, E. Aktürk, H. Sahin, and S. Ciraci, Two- and one-dimensional honeycomb structures of silicon and germanium, *Phys. Rev. Lett.* 102(23), 236804 (2009)
29. H. Nakano, T. Mitsuoka, M. Harada, K. Horibuchi, H. Nozaki, N. Takahashi, T. Nonaka, Y. Seno, and H. Nakamura, Soft synthesis of single-crystal silicon monolayer sheets, *Angew. Chem. Int. Ed.* 45(38), 6303 (2006)
30. Y. Chen, J. Xi, D. Dumcenco, Z. Liu, K. Suenaga, D. Wang, Z. Shuai, Y. S. Huang, and L. Xie, Tunable band gap photoluminescence from atomically thin transition-metal dichalcogenide alloys, *ACS Nano* 7(5), 4610 (2013)
31. S. Tongay, J. Zhou, C. Ataca, K. Lo, T. S. Matthews, J. Li, J. C. Grossman, and J. Wu, Thermally driven crossover from indirect toward direct bandgap in 2D semiconductors: $MoSe_2$ versus MoS_2, *Nano Lett.* 12(11), 5576 (2012)

32. H. Sahin, S. Tongay, S. Horzum, W. Fan, J. Zhou, J. Li, J. Wu, and F. M. Peeters, Anomalous Raman spectra and thickness-dependent electronic properties of WSe_2, *Phys. Rev. B* 87(16), 165409 (2013)
33. S. Zhang, Z. Yan, Y. Li, Z. Chen, and H. Zeng, Atomically thin arsenene and antimonene: Semimetal-semiconductor and indirect-direct band-gap transitions, *Angew. Chem. Int. Ed.* 54(10), 3112 (2015)
34. S. Zhang, M. Xie, F. Li, Z. Yan, Y. Li, E. Kan, W. Liu, Z. Chen, and H. Zeng, Semiconducting group 15 monolayers: A broad range of band gaps and high carrier mobilities, *Angew. Chem. Int. Ed.* 55(5), 1666 (2016)
35. S. Zhang, W. Zhou, Y. Ma, J. Ji, B. Cai, S. A. Yang, Z. Zhu, Z. Chen, and H. Zeng, Antimonene oxides: Emerging tunable direct bandgap semiconductor and novel topological insulator, *Nano Lett.* 17(6), 3434 (2017)
36. S. Zhang, S. Guo, Z. Chen, Y. Wang, H. Gao, J. Gómez-Herrero, P. Ares, F. Zamora, Z. Zhu, and H. Zeng, Recent progress in 2D group-VA semiconductors: From theory to experiment, *Chem. Soc. Rev.* 47, 982 (2018)
37. Y. Guo, S. Zhang, and Q. Wang, Electronic and optical properties of silicon based porous sheets, *Phys. Chem. Chem. Phys.* 16(31), 16832 (2014)
38. S. Zhang, S. Guo, Y. Huang, Z. Zhu, B. Cai, M. Xie, W. Zhou, and H. Zeng, Two-dimensional SiP: an unexplored direct band-gap semiconductor, *2D Mater.* 4, 015030 (2017)
39. Y. Ding and Y. Wang, Density functional theory study of the silicene-like SiX and XSi_3 (X = B, C, N, Al, P) Honeycomb Lattices: The various buckled structures and versatile electronic properties, *J. Phys. Chem. C* 117(35), 18266 (2013)
40. L. Zhou, Y. Guo, and J. Zhao, GeAs and SiAs monolayers: Novel 2D semiconductors with suitable band structures, *Phys. E* 95, 149 (2018)
41. C. Barreteau, B. Michon, C. Besnard, and E. Giannini, High-pressure melt growth and transport properties of SiP, SiAs, GeP, and GeAs 2D layered semiconductors, *J. Cryst. Growth* 443, 75 (2016)
42. MedeA® version 2.16. MedeA® is registered trademark of Materials Design, Inc., Angel Fire, New Mexico, USA
43. J. P. Perdew, K. Burke, and M. Ernzerhof, Generalized gradient approximation made simple, *Phys. Rev. Lett.* 77(18), 3865 (1996)
44. J. Heyd, G. E. Scuseria, and M. Ernzerhof, Hybrid functionals based on a screened Coulomb potential, *J. Chem. Phys.* 118(18), 8207 (2003)
45. G. Martyna, M. Klein, and M. Tuckerman, Nosé–Hoover chains: The canonical ensemble via continuous dynamics, *J. Chem. Phys.* 97(4), 2635 (1992)
46. M. D. Segall, P. J. D. Lindan, M. J. Probert, C. J. Pickard, P. J. Hasnip, S. J. Clark, and M. C. Payne, First-principles simulation: ideas, illustrations and the CASTEP code, *J. Phys.: Condens. Matter* 14(11), 2717 (2002)
47. H. L. Zhuang and R. G. Hennig, Single-layer group-III monochalcogenide photocatalysts for water splitting, *Chem. Mater.* 25(15), 3232 (2013)
48. V. Chakrapani, J. C. Angus, A. B. Anderson, S. D. Wolter, B. R. Stoner, and G. U. Sumanasekera, Charge transfer equilibria between diamond and an aqueous oxygen electrochemical redox couple, *Science* 318(5855), 1424 (2007)